Hindawi
Oxidative Medicine and Cellular Longevity
Volume 2022, Article ID 1548410, 12 pages
https://doi.org/10.1155/2022/1548410

Research Article

Synthesis and Characterization of a Novel Dual-Responsive Nanogel for Anticancer Drug Delivery

Darya Aminoleslami,[1] Sahar Porrang,[2] Parviz Vahedi,[3] and Soodabeh Davaran[1,4]

[1]*Research Centre for Pharmaceutical Nanotechnology, Tabriz University of Medical Sciences, Tabriz, Iran*
[2]*Chemical Engineering Faculty, Sahand University of Technology, Sahand New Town, Tabriz, Iran*
[3]*Department of Anatomical Sciences, Maragheh University of Medical Sciences, Maragheh, Iran*
[4]*Department of Medical Nanotechnology, Faculty of Advanced Medical Science, Tabriz University of Medical Sciences, Tabriz, Iran*

Correspondence should be addressed to Soodabeh Davaran; davaran@tbzmed.ac.ir

Received 15 July 2022; Accepted 3 September 2022; Published 19 September 2022

Academic Editor: Dragica Selakovic

In this study, to reduce the side effects of anticancer drugs and also to increase the efficiency of current drug delivery systems, a pH and temperature-responsive polymeric nanogel was synthesized by copolymerization of N-vinylcaprolactam (VCL) and acrylic acid (AA) monomers (P(VCL-co-AA)) with a novel cross-linker, triethylene glycol dimethacrylate (TEGDMA), as a biocompatible and nontoxic component. The structural and physicochemical features of the P(VCL-co-AA) nanogel were characterized by FT-IR, DLS/Zeta potential, FE-SEM, and ^{1}HNMR techniques. The results indicated that spherical polymeric nanogel was successfully synthesized with a 182 nm diameter. The results showed that the polymerization process continues with the opening of the carbon-carbon double bond of monomers, which was approved by C-C band removing located at 1600 cm^{-1}. Doxorubicin (Dox) as a chemotherapeutic agent was loaded into the P(VCL-co-AA), whit a significant loading of Dox (83%), and the drug release profile was investigated in the physiological and cancerous site simulated conditions. P(VCL-co-AA) exhibited a pH and temperature-responsive behavior, with an enhanced release rate in the cancerous site condition. The biocompatibility and nontoxicity of P(VCL-co-AA) were approved by MTT assay on the normal human foreskin fibroblasts-2 (HFF-2) cell line. Also, Dox-loaded P(VCL-co-AA) had excellent toxic behavior on the Michigan Cancer Foundation-7 (MCF-7) cell line as model cancerous cells. Moreover, Dox-loaded P(VCL-co-AA) had higher toxicity in comparison with free Dox, which would be a vast advantage in reducing Dox side effects in the clinical cancer treatment applications.

1. Introduction

Breast cancer is one of the most widespread cancers among women in the world for many years [1]. Surgery is one of the well-known treatments for breast cancer. By progressing in science, surgery knowledge moved from radical mastectomy to a more conservative form [2]. Although surgical treatment is not recommended for inflammatory breast cancer and recurrent and metastatic forms [2]. However, on the other hand, surgery can cause unresected tumors and increase the rates of local relapse [3]. Therefore, chemotherapy has always been used as the main cancer treatment method. Doxorubicin, as a widely used anticancer, was used to treat numerous varieties of cancers [4]. Most of pharmaceutical agents including doxorubicin have toxic effects on human body [5, 6]. Nanomedicines are becoming very popular these decades for their special properties like small size, reduced drug toxicity, controlled drug release, and ease of biological distribution [7–10]. These properties make nanomedicines be suitable method for personalized treatment in breast cancer management, although up to now no product has been registered. The use of nanomedicines such as nanogels (NGs) as drug nanocarriers is particular for making a balance between maximum therapeutic efficacy and lower toxicity [11–16]. They can control drug release in response to physiological or environmental triggers [15, 17]. NGs

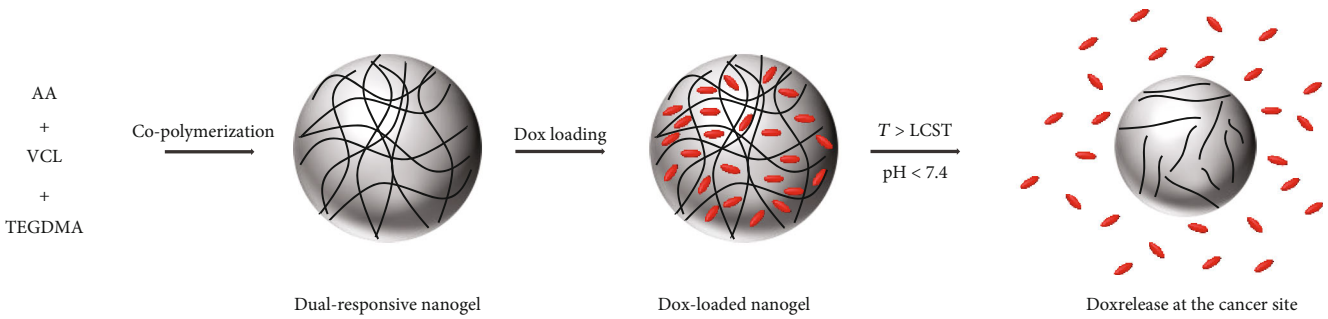

Figure 1: Synthesis process of dual-responsive P(VCL-co-AA) nanogels.

are swollen cross-linked polymer nanoparticles that can be used as highly efficient nanocarriers in controlled drug delivery [18]. Biocompatibility, stability, high surface area, easy surface modification, high cellular uptake, and unique mechanical properties are some specific features of NGs, which are important in intracellular delivery applications [19, 20]. Nanogels can be used as smart cancer treatment agents in stimulus-responsive systems category. These systems can control drug release in response to physiological or environmental triggers [12, 21]. Several stimulus-responsive polymers have been utilized for targeted drug delivery. Because of higher metabolism and inflammation [22–24] through tumor tissues, temperature-responsive polymers were introduced for cancer treatment. These polymers are sensitive to ambient temperature changes and classified according to the lower critical solution temperature (LCST). Temperature-responsive polymers are soluble and swollen at temperatures below LCST due to the formation of hydrogen bonds between the hydrophilic portions of the polymer and water molecules. However, at temperatures above LCST, they become insoluble due to the stronger reaction of the hydrophobic groups compared to hydrogen bonds [20, 25–27]. Polymer concentration, solvent auxiliaries, additives, and types of existing functional groups are among the factors affecting the polymer's LCST point. For example, if the hydrophilic groups' counts be higher than hydrophobic groups, due to the augmentation in the possibility of hydrogen bonding between the polymer and water, an increase in LCST temperature can be observed [28, 29]. Poly(N-isopropyl acrylamide) (PNIPAAm) and poly(n-vinylcaprolactam) (PVCL) are among the temperature-sensitive polymers. PNIPAAM is a polymer with a critical solubility point of about 32° C, while its LCST is nonmolecular weight dependent [30]. PVCL is also a polymer with a critical solubility point of about 32-34° C, but its LCST depends on its molecular weight, polymer concentration, and solvent composition [20, 26, 27]. One of the special properties of PVCL is its resistance to amidase enzymes, which naturally produces fewer toxic amides due to the decomposition of the polymer in its environment [19, 31, 32]. Moreover, the pH of cancerous sites is lower than physiological pH due to the high rate of glycolysis in both aerobic and anaerobic conditions. So, pH is one of the factors that can be used in targeted drug delivery [26]. Poly(acrylic acid) (PAA) and poly(methacrylic acid) (PMAA) are some kinds of pH-responsive polymers [33]. PAA responds to the pH of the environment-dependent on the ionization and deionization of the carboxylic group at different pHs [29]. PMAA is another example that changes depending on the separation of its carboxylic acid group [34].

By simultaneously using temperature and pH-responsive monomers in the nanogel structure, dual-responsive systems can be created which have controlled drug release behavior in the cancerous site. Recently, Chang et al. synthesized pH and temperature-responsive nanogels based on sodium alginate with the natural pH sensitivity and PNIPAAm as a temperature-sensitive polymer [35]. They modified sodium alginate by glutamic acid and ethylenediamine to change its charge distribution to achieve desire pH sensitivity. Then, by cross-liking NIPAAm, they could design and fabricated dual stimulus-responsive system to deliver berberine hydrochloride to the cancerous site. By changing pH and temperature NGs, networks were weakened, and the NGs collapsed to release drug rapidly. Also, the cytotoxicity test showed the low cytotoxicity and high biocompatibility [35]. Rao et al. fabricated poly(vinyl caprolactam) (PVCL) nanogels with disulfide linkages to deliver Dox for cancer treatment [36]. This system could release Dox under dual stimulus conditions, such as redox and temperature. As-mentioned nanogels were biocompatible against CCDK-skin fibroblast cells, and on the other hand, they showed high cytotoxicity against HepG2 cancer cells. Also, they could release Dox nearby nucleus by easy interrelation in the cancer cells [36]. Another pH and temperature-responsive Dox delivery system based on nanogels for cancer treatment is PNIPAAm and polyethylenemine (PEI) nanogel with magnetic graphene nanosheets as core of the system [37]. The LCST of this nanogel can be easily tuned in the range of 38–42°C. The biocompatibility and nontoxicity of the blank nanogel were confirmed against HEK293T normal and HepG2 cancerous cells and Dox loaded nanogels showed high cytotoxicity against HepG2 cell line with high cellular uptake [37].

In this research, a dual-responsive polymeric nanogel (P(VCL-co-AA)) was synthesized by free radical copolymerization of AA and VCL monomers. The synthesis process has been shown in Figure 1. Then, the P(VCL-co-AA), AA, VCL, Dox, and Dox-loaded nanogel were characterized by FT-IR. FE-SEM was used to visualize our nanogel before and after drug loading. DLS/Zeta potential technique was used to determine the particle size and distribution. Also, ^{1}HNMR analysis was taken to structural characterization of nanogel. Dox loading efficiency, Dox controlled release,

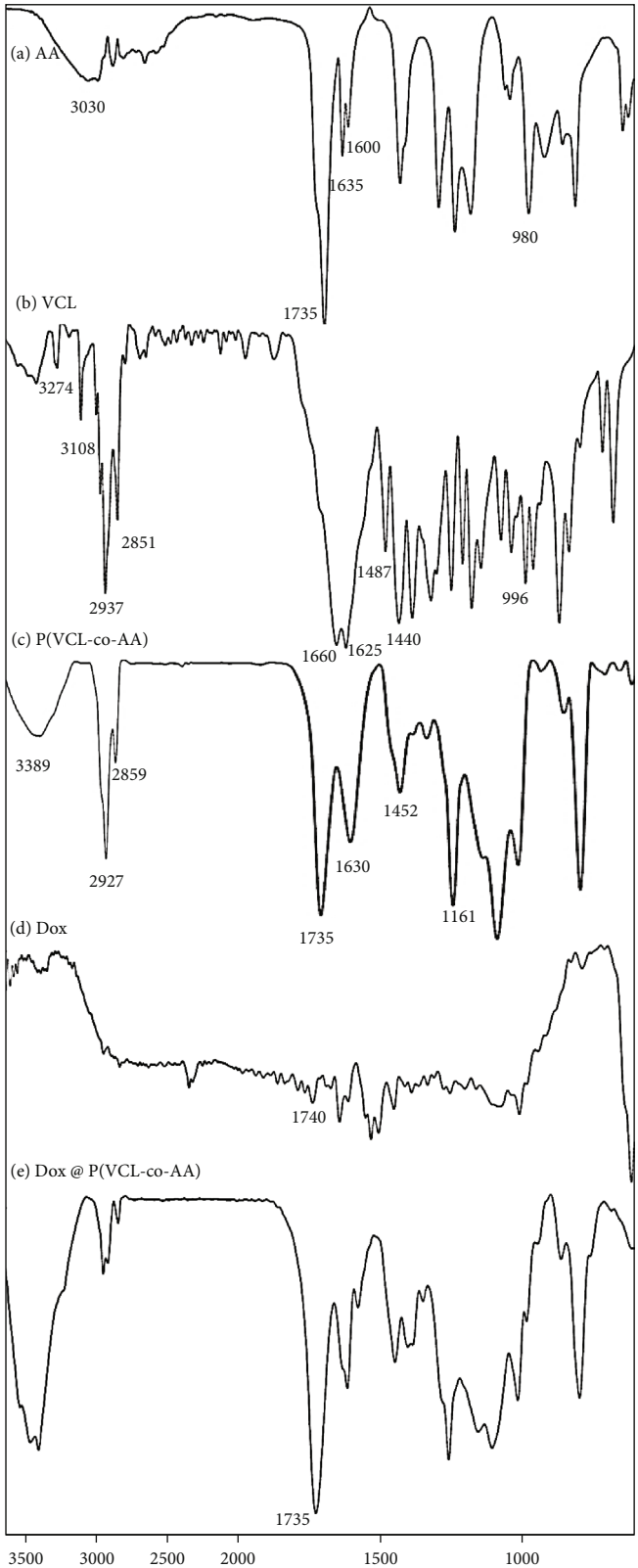

Figure 2: FT-IR spectra of (a) AA, (b) VCL, (c) P(VCL-co-AA), (d) Dox, and (e) Dox @ P(VCL-co-AA).

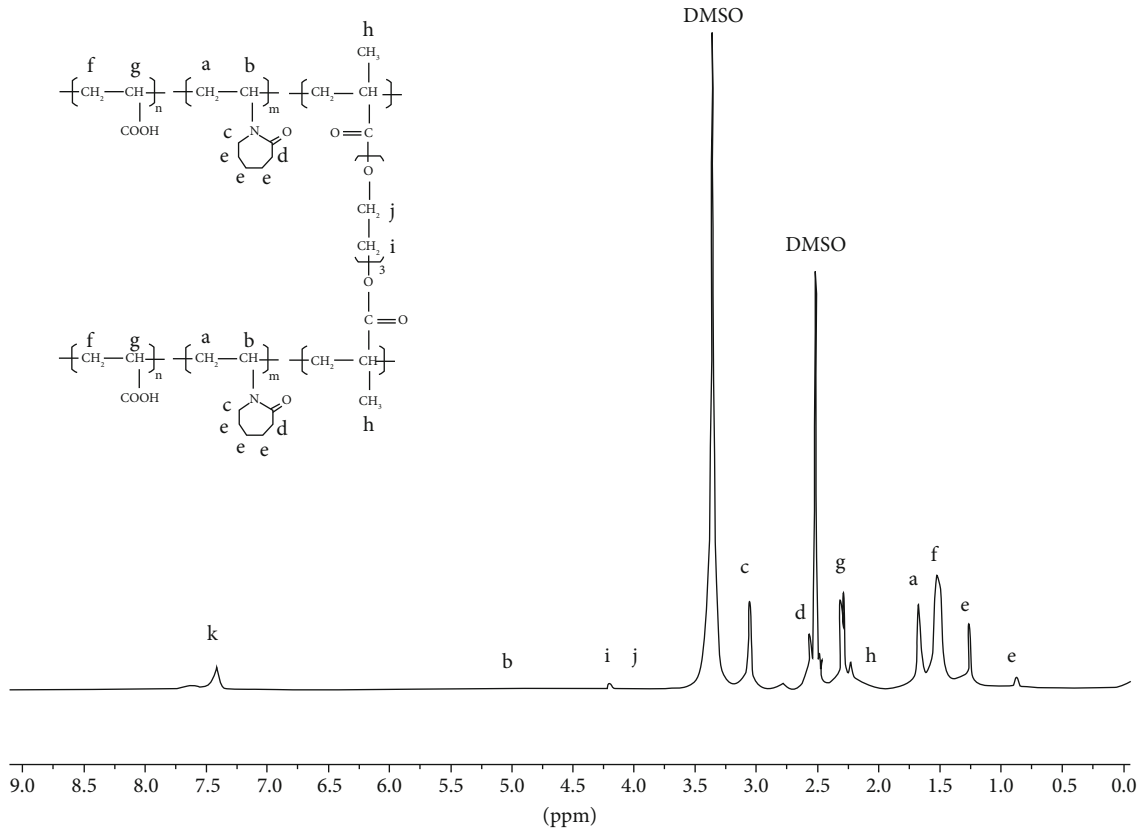

Figure 3: ^{1}H NMR spectra of the P(VCL-co-AA).

LCST, and swelling ratio of nanogel were studied to its drug delivery potential. Moreover, the biocompatibility of blank P(VCL-co-AA) against HFF-2 cell line and cytotoxicity of free Dox and Dox-loaded P(VCL-co-AA) against MCF-7 were studied by MTT assay.

2. Materials and Methods

2.1. Materials. Acrylic acid (AA) as a pH-responsive monomer, Vinylcaprolactam (VCL) as a temperature-responsive monomer, and triethylene glycol dimethacrylate (TEGDMA) were obtained from Merck Chemical Co. (Darmstadt, Germany). Potassium persulfate (KPS) was obtained from Sigma-Aldrich, Chemical Co. (St. Louis, MO USA). Sodium dodecyl sulfate (SDS) was obtained from Merck (Darmstadt, Germany). Doxorubicin (Dox) was obtained from Ebewe (Ebewe pharma, Austria). The cell culture medium (RPMI-1640), penicillin-streptomycin, and FBS were obtained from Gibco Company, Scotland. MCF-7 and HFF-2 cell lines were purchased from the Pasteur Institute, Iran. Dimethyl sulfoxide (DMSO), trypsin, and 5-diphenyl-2-H-tetrazolium bromide (MTT) were obtained from Sigma-Aldrich Chemical Co., USA.

2.2. Synthesis of Dual-Responsive Polymeric Nanogel. P(VCL-co-AA) nanogel was synthesized using TEGDMA as a cross-linker and KPS as a polymerization initiator. The P(VCL-co-AA) synthesis procedure was used. In a two-neck round bottom container, VCL (2.5 g), AA (0.075 ml), TEGMA (0.0774 g), KPS (0.425 g), and SDS (0.25 g) were dissolved in 30 ml water. Then, the mixture was purged under the nitrogen atmosphere and in an oil bath at 70°*C* for 24 h. After 24 h, we must cool it down to room temperature; then, we pass it from a filter paper then dry it in a freeze dryer.

2.3. Nanogel Characterization. Fourier transforms infrared (FT-IR) spectra of the P(VCL-co-AA), AA, VCL, Dox, Dox-loaded nanogel were taken in a Bruker tensor FT-IR (Bruker, Tensor 27, Germany). The samples were provided using potassium bromide (KBr) and then compressing the mixture to make disks. A scanning electron microscope (SEM) was used to visualize our nanogel and drug-loaded nanogel (MIRA 3 FEG-SEM, Tescan, Czech Republic). Proton nuclear magnetic resonance (1 222 H-NMR) spectra were documented at 25°C by an FT-NMR (400 MHz) Bruker spectrometer (Bruker, Ettlingen, Germany). The polymer for HNMR spectroscopy was provided by dissolving the P(VCL-co-AA) polymer in DMSO as a solvent. The average diameter and zeta potential of nanogel P(VCL-co-AA) and Dox-loaded nanogel were measured by laser-scattering technique (NanoZS ZEN 3600, Malvern Instruments, UK) before examination use of DMSO as a solvent.

2.4. Lower Critical Solution Temperature (LCST) Measurement. The LCST of nanogel was determined by the optical turbidity measurement method. A weighted amount of nanogel (0.1 g) was dissolved in buffers with various

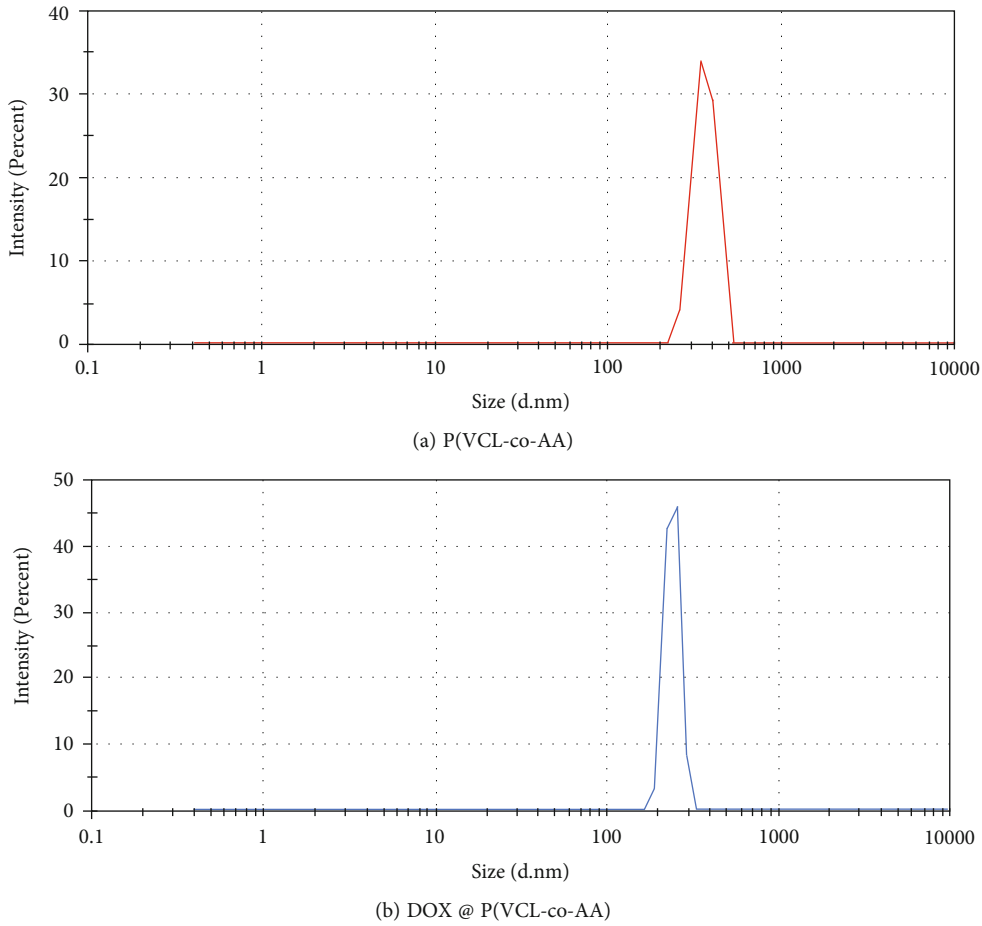

(a) P(VCL-co-AA)

(b) DOX @ P(VCL-co-AA)

Figure 4: Size distribution analysis by dynamic light scattering (DLS).

pHs (5, 7.4, 8) and the temperature was then gradually raised. The temperature at which detectable sediments were formed in the mixture was reported as nanogel LCST at relevant pH.

2.5. Swelling Ratio of P(VCL-co-AA) Measurement. For swelling ratio investigation, 0.3 g of dried nanogel was dissolved in 20 ml of water, then left for 72 hours to swell. The swelling ratio of P(VCL-co-AA) was calculated by following equation:

$$\text{Swelling ratio}\,(\%) = \frac{\text{Wt} - \text{Wd}}{\text{Wd}} * 100. \quad (1)$$

Wt is the swollen weight (gr), and Wd is the dried weight (gr).

2.6. Drug Loading into the Nanoparticles. Thirty milligrams of synthetized nanogel P(VCL-co-AA) was dispersed in 3 ml deionized water under stirring at 4°C. Then, 2.25 ml Dox solution (50 mg DOX in 25 ml deionized water) was added, and the system was stirred at 400 rpm for 24 h. After that, the drug-loaded polymer was centrifuged (6000 rpm, 10 min). Then, drug-loaded nanogel was dried in a freeze dryer. The loading percentage was determined by a spectrophotometric method (UV-Vis) at 482 nm.

2.7. In Vitro Controlled dox Release. Dox-loaded P(VCL-co-AA) was dispersed in 5 ml of PBS with different pHs (7.4 and 5.4). The vials were transmitted into a shaker incubator at temperatures about 37 and 40°C. At specified intervals, the contents of the vials were centrifuged, and the supernatant was removed and replaced with a refresh PBS. The released drug amount was determined by a UV-Vis spectrophotometer at 482 nm.

2.8. Cell Culture. Cell culture was performed according to the method previously described [23, 38]. Briefly, human foreskin fibroblast (HFF-2, normal cell) was chosen for the evaluation of biocompatibility and safety of blank P(VCL-co-AA) on normal cells. Cytotoxicity evaluation of Dox-loaded P(VCL-co-AA) was evaluated on human breast cancer cells (MCF-7). The cell lines were incubated in RPMI 1640 medium (10% (*v*/*v*) FBS and 100 U/ml penicillin) at 37°C in a 5% CO_2 humidified atmosphere [22, 39].

2.9. The In Vitro Cytotoxicity Using MTT Assay. The cytotoxicity of P(VCL-co-AA) against HFF-2 and Dox-loaded P(VCL-co-AA) cytotoxicity against MCF-7 cells was

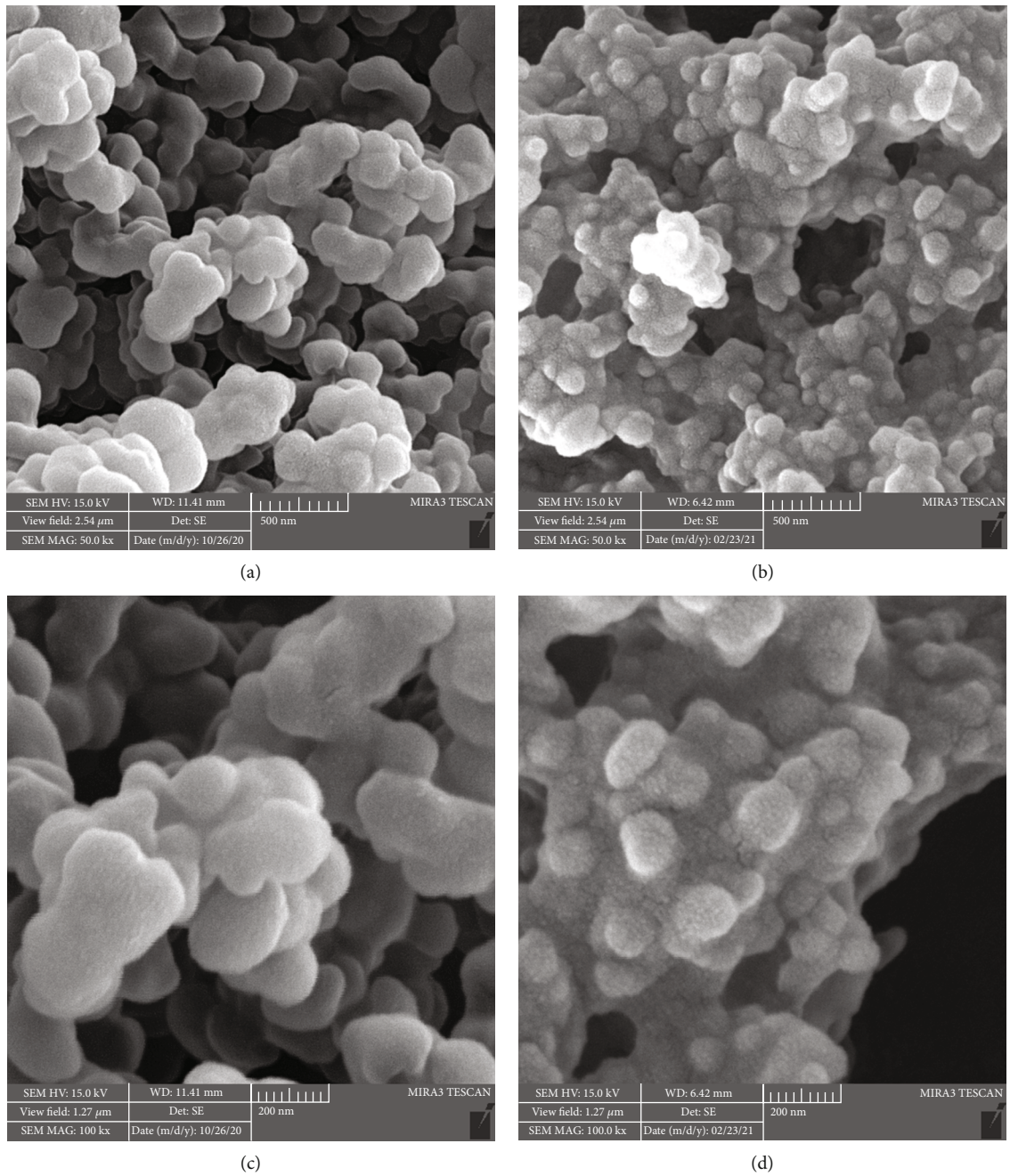

Figure 5: SEM images of P(VCL-co-AA), (a) scale bar 500, and (b) 200 nm and Dox @ P(VCL-co-AA), (c) scale bar 500, and (d) 200 nm.

assessed *in vitro*. The cells were seeded into MTT microplates (96-well) with a density of 10^4 cells/well and incubated for 24, 48, and 72 h. The HFF-2 cells were treated with blank P(VCL-co-AA) with 0.8 to 400 mg ml^{-1} concentration range. MCF-7 cells were treated with Dox-loaded P(VCL-co-AA) with concentrations ranging from 0.039 to 50 mg ml^{-1}. After the incubation time was elapsed, the contents of the wells were replaced with 20 μl MTT solution (5 mg/ml in PBS). After 3 h, the purple formazan crystals were formed. The crystals were dissolved with 100 μl DMSO. For cell viability detection, the absorbance of microplate content was assessed at 570 nm with an Elisa microplate reader. All experiments were repeated three times [39, 40].

3. Results and Discussion

3.1. Structural Characterization. In order to structure characterization of nanogel in comparison with free monomers and FTIR measurements of monomers, polymeric nanogels were obtained and are illustrated in Figures 2(a)–2(c). However, for displaying Dox existence in polymeric nanogel after drug loading, the FT-IR analysis of free Dox and Dox-loaded sample was obtained and is shown in Figures 2(d) and 2(e). There were significant differences between the prepared polymeric nanogels and the monomers. The characteristic peaks of AA related to C=O and C=C bonds were located at 1635 and 1600 cm^{-1}. After the polymerization process, as

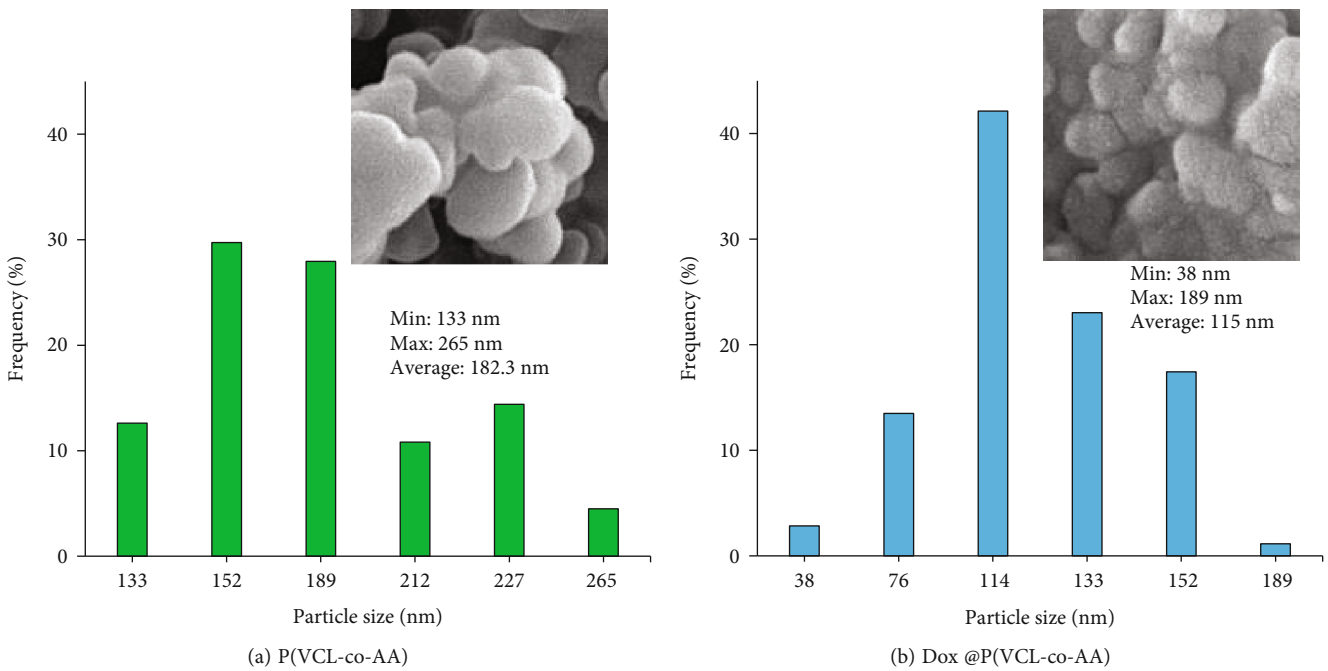

Figure 6: Particle size distribution of (a) P(VCL-co-AA) and (b) Dox-loaded P(VCL-co-AA).

Table 1: LCST points of P(VCL-co-AA) in various pHs.

pH	5	7	8
LCST (°C)	17-20	25-28	32-34

illustrated in Figure 2(c), the C=O bond was visible at a wavelength of 1635 cm^{-1} again. While the peak of the carbon-carbon double bond was removed, which indicates the successful synthesis of nanogel. Also, the peak in the wavelength of 1735 cm^{-1} has ascribed to the stretching vibration of -COOH. The broad peak from 2800 to 3500 cm^{-1} in Figures 2(a) and 1(c) is related to O-H stretching of AA carboxylic acid functional group [41]. The vibration of C-H bond due to C=C-H corresponding to AA can be seen at wavelength 980 cm^{-1} as shown in Figure 2(a). After polymerization, this peak has been removed in the FT-IR pattern, and instead, a peak is formed at 1161 cm^{-1}, which corresponds to the C-C band. As shown in Figures 1(c), O-H group vibration of acrylic acid units is revealed at wavelength 3030 cm^{-1}, in which after polymerization this peak is removed [41–43]. At the same time, the absorption peak of the C-H bond of methylene groups after polymerization is visible at 2927 cm^{-1} in the nanogel pattern [43]. Figure 2(b) shows the FT-IR spectrum of the VCL monomer. The peak generated at wavelengths of 1625 cm^{-1} corresponds to C=C, and the peak generated at 1660 cm^{-1} corresponds to the carbonyl group (C=O), which are two characteristic peaks of the VCL monomer. The peaks generated in positions 2937 cm^{-1} and 2851 cm^{-1} belong to the aliphatic C-H stretching band. At wavelength 1440 cm^{-1}, the peak corresponding to -CH_2- is displayed. The characteristic peaks of the vinyl group (=CH and =CH_2) are located at 3108 cm^{-1} and 996 cm^{-1}. Also, the peak of the C-N band is located at 1487 cm^{-1} wavelength [44]. The peak created at 3274 cm^{-1} also corresponds to the N-H band. After polymerization, as shown in Figure 2(c), the peak at position 1630 cm^{-1} belongs to the carbonyl group. The peak of the carbon-carbon double bond is also removed after polymerization. This phenomenon indicates that the polymerization process continues with the opening of the carbon-carbon double bond. The aliphatic C-H stretching is visible at wavelengths 2927 cm^{-1} and 2859 cm^{-1} as long as they were visible in the monomer patterns. The CH_2 peak is located at 1420 cm^{-1} wavelength. Also, after polymerization, the peaks of the vinyl group are removed, which indicates a successful polymerization process. The peak corresponding to the stretching vibration of C-N is located at 1452 cm^{-1}, and the peak at position 3274 cm^{-1} corresponds to the N-H band, which becomes broader in the polymer state [32, 44, 45]. Figure 2(d) shows the FT-IR profile of doxorubicin, and Figure 2(e) shows the Dox-loaded P(VCL-co-AA). In Figure 2(d), the peak created at position 1731 cm^{-1} corresponds to the C=O group of Dox. As shown in Figure 2(e), the intensity of this peak increased after the drug was loaded with P(VCL-co-AA). Also, peaks between 1400 and 1500 cm^{-1} wavelengths correspond to the doxorubicin's aromatic ring, and peaks around 1100 cm^{-1} are also related to the C-O bond [46–48]. The doxorubicin aromatic ring peaks can also be seen in the drug-loaded nanogel. The above observations indicate the successful loading of doxorubicin into the nanogel.

The ^{1}H NMR spectra of the P(VCL-co-AA) in DMSO are shown in Figure 3. The created peaks were named according to their molecular structure, as drawn in Figure 3. The protons in CH_2 (peak a) of the carbon-carbon chain of copolymer were observed at 1.65 ppm. Peak b at 5.02 ppm is related to methylene resonance which bonded with N. The proton signals at 3.2 (peak c) and

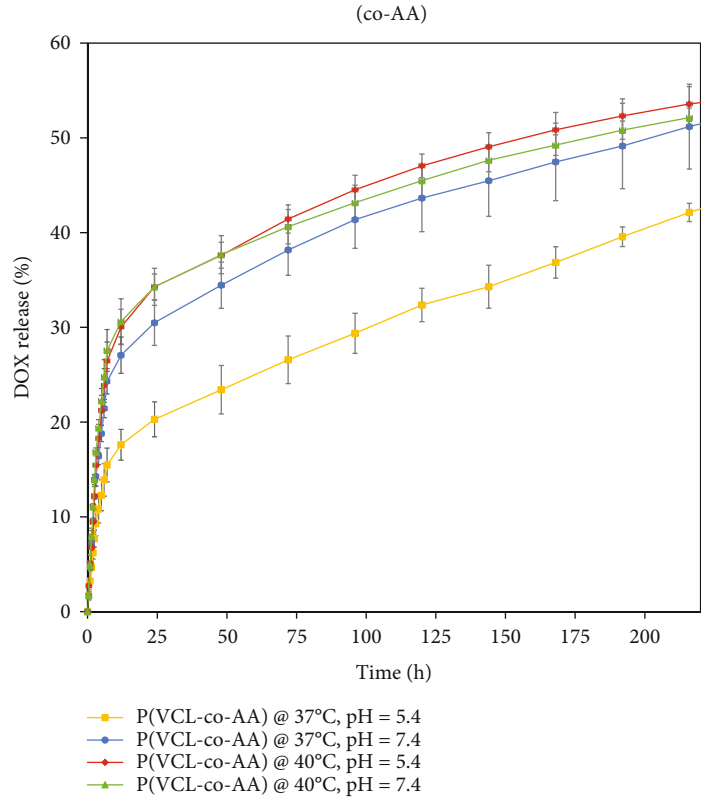

Figure 7: DOX release profile at various pH and temperature.

2.6 ppm (peak d), respectively, have belonged to methine connected with N, and methylene bonded with a carbonyl group on the heterocyclic ring. Also, protons located in the heterocyclic ring were observed at 0.85 and 1.26 ppm (peak e). Protons in CH2 (peak f) of the carbon-carbon chain of nanogel were observed at 1.51 ppm. The peak observed at 2.3 ppm (peak g) have attributed to protons in the methine group of nanogel. According to meager amount of cross-linker in the reaction mixture, however, the characteristic peaks of TEGDMA appeared as weak peaks in the 1H NMR pattern which are located at 2.07 (peak h), 4.22 (peak i), and 3.7 ppm (peak j). Also, the signal at 7.4 ppm (peak k) can be related to protons, which are created by N hydrogen banding.

4. Physicochemical and Morphological Characterization

The size and surface charge of blank and Dox-loaded polymeric nanogels were assessed with DLS and zeta potential measurements, respectively. The size distribution of P(VCL-co-AA) and Dox @ P(VCL-co-AA) is illustrated in Figure 4. DLS demonstrated that the size of blank P(VCL-co-AA) is about 798 nm, but more than five times increases in the size of nanogel after Dox loading (4575 nm). Results of zeta potential measurement match the trend seen in DLS. Blank P(VCL-co-AA) and Dox-loaded P(VCL-co-AA) have a zeta potential of -30 and -20 mV, respectively. The pKa of Dox is about 8.46, which can be protonated under neutral conditions and be a positively charged molecule [49]. So, in the presence of Dox molecules in the P(VCL-co-AA) network, the surface charge decreases to -20 mV. In this state, the repulsive force between the Dox @ P(VCL-co-AA) nanoparticles reduces, and nanoparticles become aggregate with a larger size compared to blank P(VCL-co-AA).

The FE-SEM images of P(VCL-co-AA) and Dox @ P(VCL-co-AA) were taken for morphological property investigation, which illustrated in Figures 5(a) and 4(b), respectively. The dominant morphology of nanogels was spherical. Specifically, after Dox loading in nanogel, the aggregation of nanoparticles was slightly increased, and the empty spaces between nanoparticles reduced. As mentioned previously, after positively charging doxorubicin loading, the surface charge of P(VCL-co-AA) became lower. So, the repulsive force between the Dox-loaded nanogels has been reduced, and their agglomeration has been raised. The diameter of P(VCL-co-AA) was estimated 182.3 nm. In contrast, the estimated diameter of Dox @ P(VCL-co-AA) was about 115 nm. Evidence shows that the size of nanoparticles has decreased after doxorubicin loading. It can be due to pH-responsive behavior of P(VCL-co-AA) in the presence of Dox. P(VCL-co-AA) has become compact in the presence of the positively charged Dox, which has reduced its size after loading with the Dox. In summary, after Dox loading by P(VCL-co-AA), the diameter of the polymeric nanogels becomes smaller, and their aggregation increases. It is noteworthy that the hydrodynamic size calculated from DLS was larger than that observed by SEM, due to the highly swollen

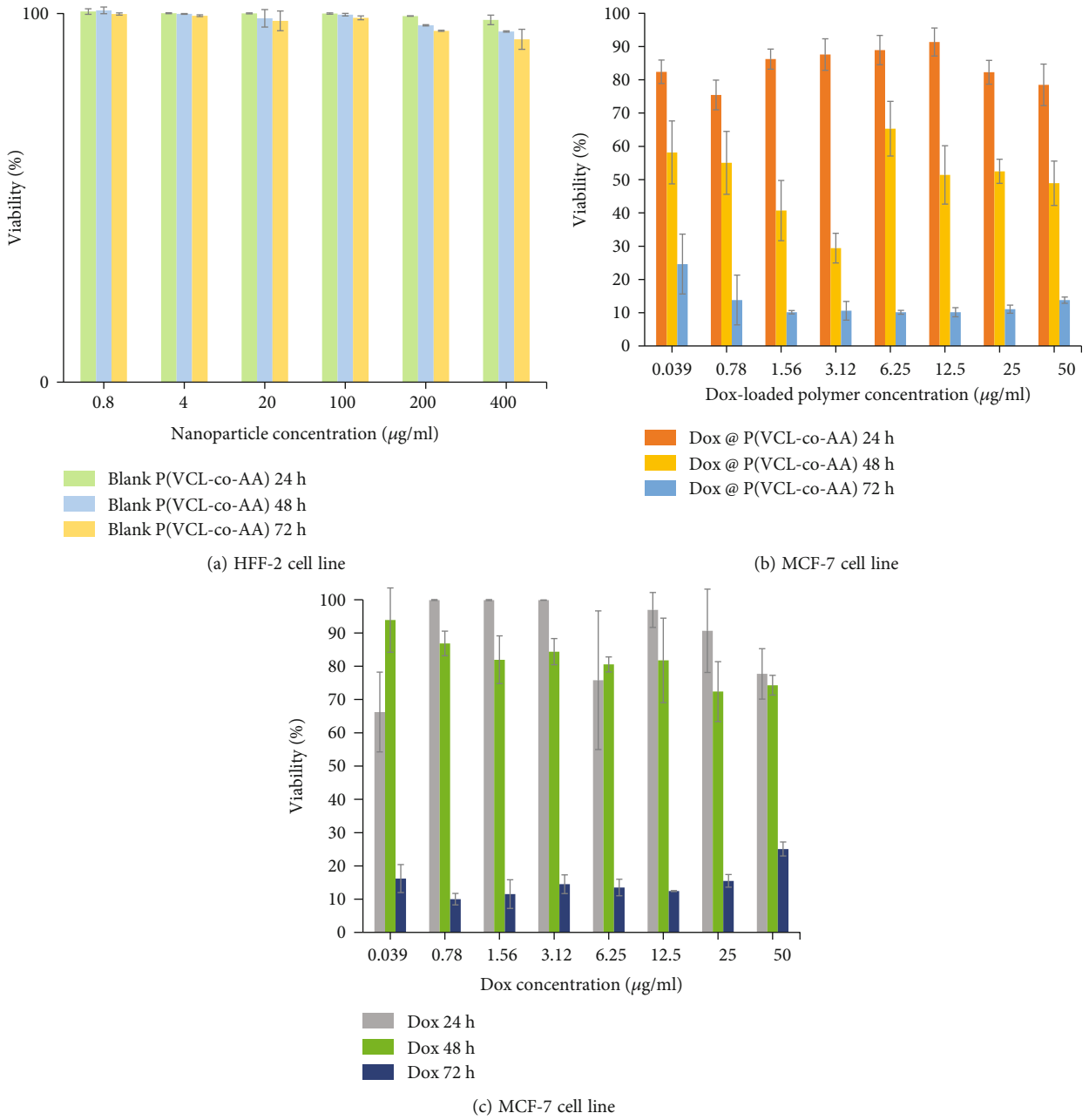

Figure 8: The cytotoxicity of (a) blank P(VCL-co-AA) to HFF-2 clell line, (b) Dox @ P(VCL-co-AA), and (c) Dox to MCF-7 cell line.

feature of P(VCL-co-AA) and Dox@P(VCL-co-AA) in an aqueous solution [50]. Moreover, they have significantly been shrunk under dry conditions [50]. The particle size distribution of P(VCL-co-AA) and Dox@P(VCL-co-AA) is illustrated in Figure 6.

4.1. LCST and Swelling Ratio of P(VCL-Co-AA). Temperature-responsive polymers are transparent at temperatures below their LCST, but as the temperature rises, the polymer collapses and the solution become turbid. The LCST point of P(VCL-co-AA) was measured by assessing the phase transition of the nanogel solution in the distilled water at different pHs (5, 7.4, and 8). The results of LCST determination are reported in Table 1. As can be derived from the results, with decreasing pH, the LCST of the nanogel also augments, and this behavior indicates the sensitivity of the nanogel to the pH. Also, P(VCL-co-AA)'s swelling ratio was determined to be 160% after floating in the water at laboratory temperature after 72 hours. All evidence suggests that the synthetic copolymer is sensitive to temperature and acidity.

4.2. In Vitro Stimulus-Responsive Drug Release. Dox as a model chemotherapeutic drug was loaded in P(VCL-co-AA) nanogel. The Dox loading percentage was about 83% which was a significant amount. Figure 7 presents the release of Dox-loaded in the P(VCL-co-AA) for 250 hours at temperatures of 37 and 40° C for pH 5.4 and 7.4. At first 12 h, Dox has bursting release. As shown in Figure 5, most drug

release has occurred under 40°C (highest temperature) and pH 5.4, which has simulated conditions for drug delivery to the tumor. According to the release profile, the release rate at pH 7.4 and 37°C was higher than pH 5.4 and 37° C. This was due to using acrylic acid monomer as a pH-sensitive agent. Due to the presence of COOH groups in the structure of polyacrylic acid, when the pH is higher than acrylic acid's pKa (4.7), these groups are ionized and become to the COO^- form, which swells by repelling each other [22, 23]. During swelling, the synthesized nanogel particles separate, and the release of the drug occurs more efficiently and faster due to the gaps created in the nanocarrier's structure. However, with the increase of temperature to 40°C, a significant rising in drug release can be observed, especially in the pH of 5.4. This behavior is due to the change in phase of the VCL polymer and temperature-responsive feature.

4.3. In Vitro Cytotoxicity Using MTT Assay. The HFF-2 cell-line was chosen to investigate the blank P(VCL-co-AA) toxicity on normal cells by MTT assay. P(VCL-co-AA) polymeric nanogel was treated with the HFF-2 cell line and incubated for 24, 48, and 72 h. As illustrated in Figure 8(a), polymeric nanogel has no significant and detectable toxicity on HFF-2 cells even in the high P(VCL-co-AA) concentrations. In previous studies, the biocompatibility of polymers resulting from the polymerization of acrylic acid and vinyl caprolactam monomers was confirmed. The results of this study also confirmed the biocompatibility of TEGDMA cross-linker. Figure 8(b) illustrates the cytotoxicity of drug-loaded P(VCL-co-AA) on the MCF-7 cell line at concentrations ranging from 0.039 to 50 $\mu g\,mL^{-1}$ for 48, 24, and 72 hours. By Dox concentration increment, the MCF-7 cells' viability decreased, and with increasing incubation time, the toxicity of Dox-loaded P(VCL-co-AA) augmented. So, Dox-loaded P(VCL-co-AA) at different incubation times has concentration-dependent toxic effects on MCF-7 cell line, which indicates the release of the drug from the designed drug delivery system under cancerous site condition. As can be seen in Figure 8(c), with free Dox concentration augment, the cell viability decreases, and with increasing incubation time, the toxicity of the drug on cells rises. For example, the vital activity of the cells at a concentration of 50 $\mu g\,ml^{-1}$ is 77.7% at 24 hours of incubation time, 74% at 48 hours of incubation time, and 25% at 72 hours of incubation time. Comparing Figures 8(b) and 7(c), it can be concluded that in all three time periods, the toxicity of the Dox-loaded P(VCL-co-AA) is higher than that of free Dox, which indicates the high efficiency of the synthesized nanogel. Enhanced toxicity of Dox-loaded P(VCL-co-AA) on MCF-7 cell line compared to the free Dox would be a massive benefit in reducing the drug dose and its side effects in the clinical cancer treatment applications.

5. Conclusion

The results this research have shown that the dual responsive cross-linked P(VCL-co-AA) nanogel can be synthesized through the free radical copolymerization-crosslinking method with a high yield. The copolymer obtained has a nanogel structure.

The characteristic properties of the nanogel were investigated by FT-IR, H-NMR, SEM, and DLS analysis, which confirmed the successful synthesis with suitable physicochemical properties. This system showed a significant loading of Dox (83%). Release in the simulated tumor area was higher than physiological conditions. The biocompatibility of nanogel was proved by MTT assay on HFF-2 cell line. The *in vitro* cytotoxicity evaluations of Dox-loaded P(VCL-co-AA) nanogel on MCF-7 cell line showed high cytotoxic effect compared to free drug. In general, these characteristics indicate the high efficiency of this specially designed smart drug delivery system for treatment of breast cancer.

5.1. Future Perspectives. The existence of some marketed formulation of nanogels shows the effective and successful performance of this class of nanocarriers in pharmaceuticals for preclinical and clinical applications. However, there are a number of inadequacies for their scale-up that future research should address. Development of a cost-effective and stable procedure for repeatable synthesis of nanogels is essential for their future marketable application. Therefore, despite the huge progress in creating stimulus-responsive nanogels for cancer treatment, still a lot of work is required to be done for their scaling up.

Abbreviation

AA: Acrylic acid
DLS: Dynamic light scattering
EE: Encapsulation Efficacy
FBS: Fetal Bovine Serum
FE-SEM: Field Emission Scanning Electron Microscopes
FT-IR: Fourier Transform-Infrared Spectroscopy
^{1}HNMR: Hydrogen-Nuclear Magnetic Resonance
IC_{50}: Inhibitory Concentration of 50%
LCST: Lower critical solution temperature
NIPAM: N-Isopropyl acryl amide
NG: Nanogel
VCL: Vinylcaprolactam
TEGDMA: Polyethylene glycol dimethacrylate
KPS: Potassium peroxydisulfate
SEM: Scanning Electron Microscopy
SDS: Sodium dodecyl sulfate
DMSO: Dimethyl sulfoxide.

Data Availability

All data used to support the findings of this study are included in the article.

Conflicts of Interest

The authors declare no conflicts of interest regarding the publication of this paper.

Acknowledgments

The authors are thankful to Tabriz University of Medical Sciences, for providing all necessary research facilities and moral supports to carry out this research.

References

[1] S. Tabatabaeian, S. Sadeghi, and H. Tabatabaeian, "PTBP1 correlates with HER2 positivity, lymph node spread and metastasis in breast cancer," *Gene Reports*, vol. 19, p. 100659, 2020.

[2] M. P. Nigdelis, M. V. Karamouzis, M. Kontos, A. Alexandrou, D. G. Goulis, and I. Lambrinoudaki, "Updates on the treatment of invasive breast cancer: *Quo Vadimus*?," *Maturitas*, vol. 145, pp. 64–72, 2021.

[3] Q. T. Shubhra, K. Guo, Y. Liu, M. Razzak, M. Serajum Manir, and A. K. M. Moshiul Alam, "Dual targeting smart drug delivery system for multimodal synergistic combination cancer therapy with reduced cardiotoxicity," *Acta Biomaterialia*, vol. 131, pp. 493–507, 2021.

[4] H. M. Alkreathy, M. H. Alkhatib, S. A. al Musaddi, K. S. A. Balamash, N. N. Osman, and A. Ahmad, "Enhanced antitumour activity of doxorubicin and simvastatin combination loaded nanoemulsion treatment against a Swiss albino mouse model of Ehrlich ascites carcinoma," *Clinical and Experimental Pharmacology and Physiology*, vol. 46, no. 5, pp. 496–505, 2019.

[5] C. S. Abdullah, S. Alam, R. Aishwarya et al., "Doxorubicin-induced cardiomyopathy associated with inhibition of autophagic degradation process and defects in mitochondrial respiration," *Scientific Reports*, vol. 9, no. 1, pp. 1–20, 2019.

[6] A. Eftekhari, E. Ahmadian, Y. Azarmi, A. Parvizpur, J. K. Fard, and M. A. Eghbal, "The effects of cimetidine, N-acetylcysteine, and taurine on thioridazine metabolic activation and induction of oxidative stress in isolated rat hepatocytes," *Pharmaceutical Chemistry Journal*, vol. 51, no. 11, pp. 965–969, 2018.

[7] S. M. Aberoumandi, M. Mohammadhosseini, E. Abasi et al., "An update on applications of nanostructured drug delivery systems in cancer therapy: a review," *Artificial Cells, Nanomedicine, and Biotechnology*, vol. 45, no. 6, pp. 1058–1068, 2017.

[8] E. Ahmadian, A. Eftekhari, T. Kavetskyy, A. Y. Khosroushahi, V. A. Turksoy, and R. Khalilov, "Effects of quercetin loaded nanostructured lipid carriers on the paraquat- induced toxicity in human lymphocytes," *Pesticide Biochemistry and Physiology*, vol. 167, p. 104586, 2020.

[9] A. Eftekhari, A. Arjmand, A. Asheghvatan et al., "The potential application of magnetic nanoparticles for liver fibrosis theranostics," *Frontiers in Chemistry*, vol. 9, p. 674786, 2021.

[10] A. Eftekhari, S. Maleki Dizaj, E. Ahmadian et al., "Application of advanced nanomaterials for kidney failure treatment and regeneration," *Materials*, vol. 14, no. 11, p. 2939, 2021.

[11] D. Bartusik-Aebisher, G. Chrzanowski, Z. Bober, and D. Aebisher, "An analytical study of trastuzumab-dendrimer-fluorine drug delivery system in breast cancer therapy *in vitro*," *Biomedicine & Pharmacotherapy*, vol. 133, p. 111053, 2021.

[12] H. J. Han, C. Ekweremadu, and N. Patel, "Advanced drug delivery system with nanomaterials for personalised medicine to treat breast cancer," *Journal of Drug Delivery Science and Technology*, vol. 52, pp. 1051–1060, 2019.

[13] S. Ehsanimehr, P. Najafi Moghadam, W. Dehaen, and V. Shafiei-Irannejad, "Synthesis of pH-sensitive nanocarriers based on polyacrylamide grafted nanocrystalline cellulose for targeted drug delivery to folate receptor in breast cancer cells," *European Polymer Journal*, vol. 150, p. 110398, 2021.

[14] J. Li, M. Li, L. Tian et al., "Facile strategy by hyaluronic acid functional carbon dot-doxorubicin nanoparticles for CD44 targeted drug delivery and enhanced breast cancer therapy," *International Journal of Pharmaceutics*, vol. 578, p. 119122, 2020.

[15] B. Ozlu, G. Kabay, I. Bocek et al., "Controlled release of doxorubicin from polyethylene glycol functionalized melanin nanoparticles for breast cancer therapy: Part I. Production and drug release performance of the melanin nanoparticles," *International Journal of Pharmaceutics*, vol. 570, article 118613, 2019.

[16] E. Ahmadian, D. Janas, A. Eftekhari, and N. Zare, "Application of carbon nanotubes in sensing/monitoring of pancreas and liver cancer," *Chemosphere*, vol. 302, p. 134826, 2022.

[17] F. Abedi, S. Davaran, M. Hekmati, A. Akbarzadeh, B. Baradaran, and S. V. Moghaddam, "An improved method in fabrication of smart dual-responsive nanogels for controlled release of doxorubicin and curcumin in HT-29 colon cancer cells," *Journal of Nanobiotechnology*, vol. 19, no. 1, pp. 1–22, 2021.

[18] J. Kousalová and T. Etrych, "Polymeric nanogels as drug delivery systems," *Physiological Research*, vol. 67, Suppl 2, pp. S305–S317, 2018.

[19] K. M. Rao, K. S. V. K. Rao, and C.-S. Ha, "Stimuli responsive poly (vinyl caprolactam) gels for biomedical applications," *Gels*, vol. 2, no. 1, p. 6, 2016.

[20] M. Camara, J. Xu, T. Ding et al., "Molecular dynamics study of the thermosensitive properties of poly (N-vinyl caprolactam) in water," *Fluid Phase Equilibria*, vol. 527, p. 112831, 2021.

[21] E. Ahmadian, S. M. Dizaj, A. Eftekhari et al., "The potential applications of hyaluronic acid hydrogels in biomedicine," *Drug Research*, vol. 70, no. 1, pp. 6–11, 2020.

[22] S. Porrang, N. Rahemi, S. Davaran, M. Mahdavi, and B. Hassanzadeh, "Synthesis of temperature/pH dual-responsive mesoporous silica nanoparticles by surface modification and radical polymerization for anti-cancer drug delivery," *Colloids and Surfaces A: Physicochemical and Engineering Aspects*, vol. 623, p. 126719, 2021.

[23] S. Porrang, N. Rahemi, S. Davaran, M. Mahdavi, B. Hassanzadeh, and A. M. Gholipour, "Direct surface modification of mesoporous silica nanoparticles by DBD plasma as a green approach to prepare dual-responsive drug delivery system," *Journal of the Taiwan Institute of Chemical Engineers*, vol. 123, pp. 47–58, 2021.

[24] M. Ashrafizadeh, H. Saebfar, M. H. Gholami et al., "Doxorubicin-loaded graphene oxide nanocomposites in cancer medicine: stimuli-responsive carriers, co-delivery and suppressing resistance," *Expert Opinion on Drug Delivery*, vol. 19, no. 4, pp. 355–382, 2022.

[25] S. Hajebi, N. Rabiee, M. Bagherzadeh et al., "Stimulus-responsive polymeric nanogels as smart drug delivery systems," *Acta Biomaterialia*, vol. 92, pp. 1–18, 2019.

[26] M. A. Rahim, N. Jan, S. Khan et al., "Recent advancements in stimuli responsive drug delivery platforms for active and passive cancer targeting," *Cancers*, vol. 13, no. 4, p. 670, 2021.

[27] N. K. Preman, R. R. Barki, A. Vijayan, S. G. Sanjeeva, and R. P. Johnson, "Recent developments in stimuli-responsive polymer nanogels for drug delivery and diagnostics: a review,"

European Journal of Pharmaceutics and Biopharmaceutics, vol. 157, pp. 121–153, 2020.

[28] M. L. Ohnsorg, J. M. Ting, S. D. Jones, S. Jung, F. S. Bates, and T. M. Reineke, "Tuning PNIPAm self-assembly and thermoresponse: roles of hydrophobic end-groups and hydrophilic comonomer," *Polymer Chemistry*, vol. 10, no. 25, pp. 3469–3479, 2019.

[29] A. Okudan and A. Altay, "Investigation of the effects of different hydrophilic and hydrophobic comonomers on the volume phase transition temperatures and thermal properties of N-isopropylacrylamide-based hydrogels," *International Journal of Polymer Science*, vol. 2019, Article ID 7324181, 12 pages, 2019.

[30] Y. Hiruta, "Poly(*N*-isopropylacrylamide)-based temperature- and pH-responsive polymer materials for application in biomedical fields," *Polymer Journal*, vol. 54, pp. 1–12, 2022.

[31] M. N. Mohammed, K. B. Yusoh, and J. H. B. H. Shariffuddin, "Poly (N-vinyl caprolactam) thermoresponsive polymer in novel drug delivery systems: a review," *Materials Express*, vol. 8, no. 1, pp. 21–34, 2018.

[32] M. Fallon, S. Halligan, R. Pezzoli, L. Geever, and C. Higginbotham, "Synthesis and characterisation of novel temperature and pH sensitive physically cross-linked poly (N-vinylcaprolactam-co-itaconic acid) hydrogels for drug delivery," *Gels*, vol. 5, no. 3, p. 41, 2019.

[33] Z. Li, J. Huang, and J. Wu, "pH-sensitive nanogels for drug delivery in cancer therapy," *Biomaterials Science*, vol. 9, no. 3, pp. 574–589, 2021.

[34] W.-X. Hong, V. Y. Shevtsov, and Y.-T. Shieh, "Preparation of pH-responsive poly (methyl methacrylate) nanoparticles with CO_2-triggered aggregation," *Journal of Polymer Research*, vol. 29, no. 8, pp. 1–13, 2022.

[35] S. Chang, D. Qin, R. Yan et al., "Temperature and pH dual responsive nanogels of modified sodium alginate and NIPAM for berberine loading and release," *ACS Omega*, vol. 6, no. 2, pp. 1119–1128, 2021.

[36] K. M. Rao, M. Suneetha, D. V. Kumar, H. J. Kim, Y. J. Seok, and S. S. Han, "Dual responsive poly (vinyl caprolactam)-based nanogels for tunable intracellular doxorubicin delivery in cancer cells," *Pharmaceutics*, vol. 14, no. 4, p. 852, 2022.

[37] S. C. Kunene, K. S. Lin, M. T. Weng, M. J. Carrera Espinoza, and C. M. Wu, "*In vitro* study of doxorubicin-loaded thermo- and pH-tunable carriers for targeted drug delivery to liver cancer cells," *Journal of Industrial and Engineering Chemistry*, vol. 104, pp. 93–105, 2021.

[38] E. Ahmadian, A. Eftekhari, H. Babaei, A. M. Nayebi, and M. A. Eghbal, "Anti-cancer effects of citalopram on hepatocellular carcinoma cells occur via cytochrome C release and the activation of NF-kB," *Anti-Cancer Agents in Medicinal Chemistry (Formerly Current Medicinal Chemistry-Anti-Cancer Agents)*, vol. 17, no. 11, pp. 1570–1577, 2017.

[39] S. Porrang, N. Rahemi, S. Davaran, M. Mahdavi, and B. Hassanzadeh, "Preparation and in-vitro evaluation of mesoporous biogenic silica nanoparticles obtained from rice and wheat husk as a biocompatible carrier for anti-cancer drug delivery," *European Journal of Pharmaceutical Sciences*, vol. 163, p. 105866, 2021.

[40] E. Ahmadian, H. Babaei, A. Mohajjel Nayebi, A. Eftekhari, and M. A. Eghbal, "Mechanistic approach for toxic effects of bupropion in primary rat hepatocytes," *Drug Research*, vol. 67, no. 4, pp. 217–222, 2017.

[41] X. Yi, Z. Xu, Y. Liu, X. Guo, M. Ou, and X. Xu, "Highly efficient removal of uranium (VI) from wastewater by polyacrylic acid hydrogels," *RSC Advances*, vol. 7, no. 11, pp. 6278–6287, 2017.

[42] X. Hu, W. Wei, X. Qi et al., "Preparation and characterization of a novel pH-sensitive salecan-g-poly (acrylic acid) hydrogel for controlled release of doxorubicin," *Journal of Materials Chemistry B*, vol. 3, no. 13, pp. 2685–2697, 2015.

[43] L. Feng, H. Yang, X. Dong, H. Lei, and D. Chen, "pH-sensitive polymeric particles as smart carriers for rebar inhibitors delivery in alkaline condition," *Journal of Applied Polymer Science*, vol. 135, no. 8, p. 45886, 2018.

[44] S. Kozanoğlu, T. Özdemir, and A. Usanmaz, "Polymerization of N-vinylcaprolactam and characterization of poly (N-vinylcaprolactam)," *Journal of Macromolecular Science, Part A*, vol. 48, no. 6, pp. 467–477, 2011.

[45] M. A. Macchione, C. Guerrero-Beltrán, A. P. Rosso et al., "Poly(N-vinylcaprolactam) nanogels with antiviral behavior against HIV-1 infection," *Scientific Reports*, vol. 9, no. 1, pp. 1–10, 2019.

[46] X. Li, C. Gao, Y. Wu, C. Y. Cheng, W. Xia, and Z. Zhang, "Combination delivery of adjudin and doxorubicin via integrating drug conjugation and nanocarrier approaches for the treatment of drug-resistant cancer cells," *Journal of Materials Chemistry B*, vol. 3, no. 8, pp. 1556–1564, 2015.

[47] F. Mohammad and N. A. Yusof, "Doxorubicin-loaded magnetic gold nanoshells for a combination therapy of hyperthermia and drug delivery," *Journal of Colloid and Interface Science*, vol. 434, pp. 89–97, 2014.

[48] R. Ganassin, C. Merker, M. C. Rodrigues et al., "Nanocapsules for the co-delivery of selol and doxorubicin to breast adenocarcinoma 4T1 cells *in vitro*," *Artificial Cells, Nanomedicine, and Biotechnology*, vol. 46, no. 8, pp. 2002–2012, 2018.

[49] A. Aziz, Y. Sefidbakht, S. Rezaei, H. Kouchakzadeh, and V. Uskoković, "Doxorubicin-loaded, pH-sensitive albumin nanoparticles for lung cancer cell targeting," *Journal of Pharmaceutical Sciences*, vol. 111, no. 4, pp. 1187–1196, 2022.

[50] Z. Wang, X. Li, X. Zhang et al., "Novel contact lenses embedded with drug-loaded Zwitterionic nanogels for extended ophthalmic drug delivery," *Nanomaterials*, vol. 11, no. 9, p. 2328, 2021.